Impedance Control of Flush-Mounted Piezoelectric Cells for Vibration and Noise Reduction in Aerodynamic Profiles Applications

Jonathan Rodriguez, Mouhamed Mounibe Ezzine, Vincent Clair, Matthias Perez, Manuel Collet

Impedance Control of Flush-Mounted Piezoelectric Cells for Vibration and Noise Reduction in Aerodynamic Profiles Applications

Jonathan Rodriguez[a], Mouhamed Mounibe Ezzine[a], Vincent Clair[a], Matthias Perez[a], and Manuel Collet[a]

[a]Univ. Lyon, Ecole Centrale de Lyon, Laboratoire de Tribologie et Dynamique des Systèmes (LTDS), UMR CNRS 5513, F-69134 Ecully, France

ABSTRACT

Methods and technologies to control the vibrations and noise on profiles excited dynamically by a fluid flow like vanes, rotor blades, or plane wings are tremendously needed. The following manuscript relies on a preliminary research proposing a vibration and noise control system integrated into the lower and upper profile of an outer guide vane prototype, consisting of five flush-mounted piezoelectric cells. To control the piezoelectric transducers, an impedance control circuit has been designed to dissociate current and voltage, and control directly their complex impedance as a frequency-dependent function. Then, the negative capacitance control principle is used to synthesize the controller as it avoids complex identification methods of the structure. Only by determining the optimal negative capacitance, it is possible to control the vibration level and acoustic transmission of the profile on a bandwidth around the main vibration mode of each cell. Hence, an average reduction level of $-6dB$ is achieved on the vibration and acoustic transmission level for a large bandwidth around $3500Hz$ and $4500Hz$, confirming the performance of negative capacitance control with the advantage of not needing the usual complex identification process of the structure model.

Keywords: impedance control, vibration control, piezoelectric transducers

1. INTRODUCTION

Aerodynamic profiles like vanes, rotor and turbine blades, or plane wings are often subject to strong vibrations and noise transmission due to turbulent airflow excitation. Thus, passive or active systems to control and limit the vibration and noise level are essential, especially for transportation applications to prevent discomfort or structural damage in more severe cases.

However, using soft materials to add damping to the structure in this type of application is not often possible since static pressure has to be maintained on both the lower and upper sides of the considered profile for functional purposes. Besides, the weight and integration of such vibration and noise control systems are also very important since the possibilities are in general very limited in blades and vanes.

Thus, piezoelectric transducers have been widely used to control structural vibrations due to their lightweight, reduced volume, and broadband control capabilities. Different passive electrical shunt strategies have been explored[1,2] based on the classical electrical components: resistance, inductance, and capacitance.

Resonant shunt damping circuits[3] have often been used for their damping performance and stability characteristics. Regarding fan blades, Hohl et al.[4] and Duffy et al.[5] for instance experimented different damping strategies using electrical shunt techniques with macro fiber composite piezoceramics located at the surface of the metallic or composite blades. However, if good damping ratios are achieved through resonant shunts, they remain quite sensitive to small variations in the structural mode frequencies. The optimal reduction can only be achieved if the shunt circuit is very precisely tuned to the frequency of the target mode. Besides, adaptive shunt damping displays better attenuation performances but increases drastically the system complexity.

Further author information: (Send correspondence to Jonathan Rodriguez)
E-mail: jonathan.rodriguez@ec-lyon.fr, Telephone: +336 2519 8054

To reduce the implementation complexity and improve the control robustness to parametric uncertainties in the structural mode frequencies, the negative capacitance shunt principle has also been investigated to control vibrations[6,7,8] with piezoelectric transducers and noise reflection.[9] This active shunt method is known to provide good performance with little dependence on structural resonance frequencies. However, negative capacitor controllers are sensitive to variations in the transducer capacitance.

Hence, the following manuscript proposes a preliminary research work on the design and control of multiple flush-mounted piezoelectric cell prototypes for vibration and noise control on aerodynamic profiles. The actual control concept is based on active impedance control and uses the negative capacitance shunt principle. In addition, the mechanical design of the cells has been optimized to take advantage of their main structural mode to control within the desired bandwidth the vibration and noise generated by the profile with maximum performance and robustness to the structural modes uncertainties.

The manuscript is organized as follows: Section 2 presents the prototype design with its electro-mechanical behavior. Section 3 develops the control method and the controllers synthesis. Finally, Section 4 addresses the experimental results obtained in vibration and emitted noise control.

2. SYSTEM DESIGN

The following Section presents the system prototype mechanical design initiated in[10] and the electro-mechanical behaviour of the cells.

2.1 Experimental system overview

The designed system is aimed to reduce the vibrations and the transmitted noise on aerodynamic profiles due to turbulent airflow in contact with the airfoil surface as illustrated in Figure 1. Each of the blue rectangles represents one piezoelectric cell whose architecture is detailed in Figure 2. Each cell is constituted by a thin $1mm$ aluminum skin of $44 \times 44mm$ with 6 transducers fixed with epoxy resin and connected in series. The transducers are PZT-5A piezoelectric patches of $2 \times 2mm$ width in the deformation direction (d_{33}).

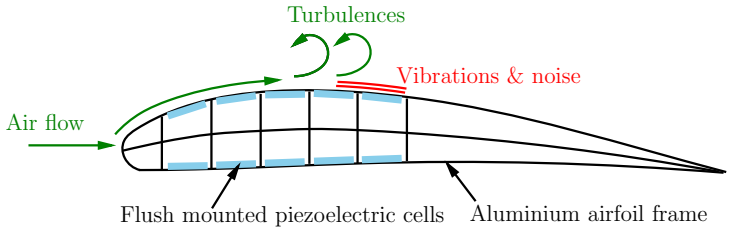

Figure 1: Active vibration and noise control system principle for aerodynamic profile.

The actual manufactured prototype of the outer vane profile consists of 5 flush-mounted piezoelectric cells to be installed in a wind-tunnel for preliminary experiments as displayed in Figure 3.

Piezoelectric shunts are usually realized using passive components. In the case of negative capacitor controllers, operational amplifiers[7] are needed to obtain a negative impedance. In our case, a dedicated active circuit has been designed such that a control input signal [V] can drive a current source [A] connected to the piezoelectric transducers (Howland current source). Since the electronic board output is the transducers voltage, it is possible then to actively control the transfer function between the transducers current and voltage *i.e* their impedance. Thus, the impedance controller is not attached to any hardware configuration and can be freely designed.

2.2 Electro-mechanical behavior

Now the electro-mechanical behavior of the cells is investigated to determine the bandwidth of maximal authority for the control. The prototype is suspended and dynamically excited by an electrodynamic shaker with a band-limited white noise at a sampling frequency of 50kHz. A laser vibrometer PSV400 measures the velocity at the

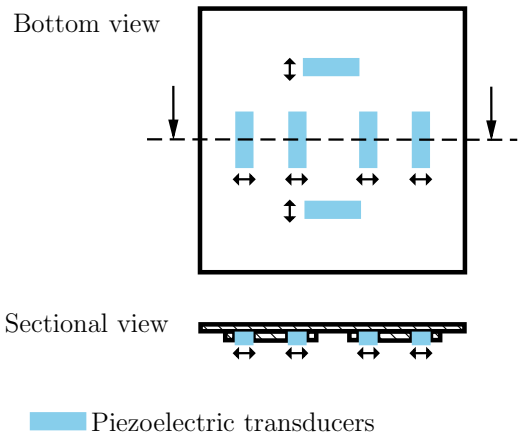

Figure 2: Schematic representation of the piezoelectric transducers implementation on each cell

center of each cell. The measured frequency response functions (FRF) and spectral coherences are displayed in Figure 4.

One can notice immediately in Figure 4a that the bandwidth of maximum authority for the control is located in frequency between 3kHz and 4kHz for the cells #1 to #4, and around 5kHz for the cell #5 which is confirmed by the spectral coherence in Figure 4b. These differences between the cell's frequency response can be explained by small discrepancies in the boundary conditions of their aluminum skin (assembly process, tightening torques, etc...), the bonding conditions of each transducer, and small uncertainties on their nominal capacitance.

Then, the prototype is dynamically excited through its 5 control inputs on the impedance control circuit with the same band-limited white noise at 50kHz. This time, the laser vibrometer measures the velocity field at the surface of each piezoelectric cell to ensure the mode shape associated with the maximum displacement bandwidth of the cell skin is compatible with a potential vibroacoustic application *i.e* displaying a piston mode. Thus, the measured velocity field is presented in Figure 5 for the bandwidth $[2500 - 5500]Hz$. The cells #1 #2, and #3 display a good velocity profile, especially the cell#2. In comparison, the electromechanical coupling for cell #4 appears weaker and the vibration shape of #5 confirms a potential problem in the boundary conditions.

3. CONTROL DESIGN

This Section develops the steps leading to the controller synthesis based on the negative capacitance principle.

3.1 Negative capacitance control

The idea behind the chosen control method is to use every piezoelectric cell as both a sensor and an actuator by controlling its impedance *i.e* the transfer function between the voltage (cell output) and the current (cell input) using a Howland current source.

Let us consider a simple model for a piezoelectric cell connected to a mechanical structure as in Figure 6. Then, the coupled electro-mechanical system is driven by the following equations:

$$m\ddot{x} + kx + c\dot{x} + \theta V_p = F \quad (1)$$

$$-\theta\dot{x} + C_p\dot{V}_p = -i \quad (2)$$

where m is the system mass, k the stiffness, c the damping coefficient, F the external force and x the mass displacement. For the electrical part, θ is the electro-mechanical coupling coefficient, C_p the transducer capacitance, V_p the transducer voltage and i the current in the circuit. Finally, Z is the shunt circuit impedance (see Figure 6).

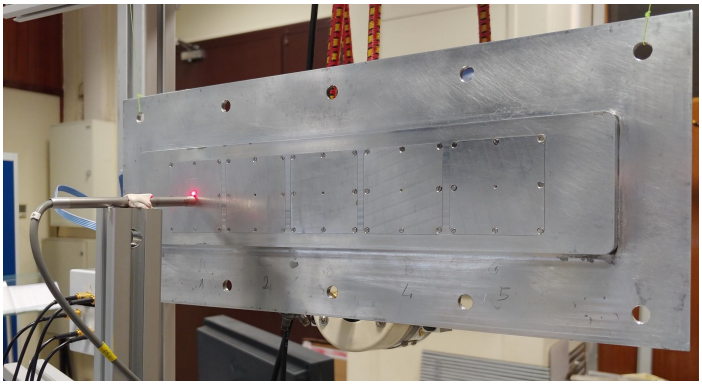

(a)

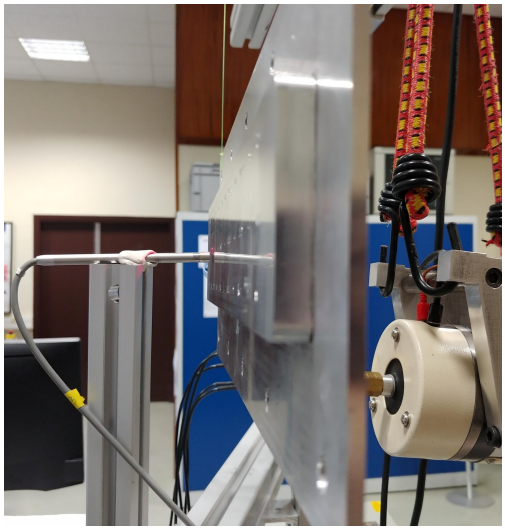

(b)

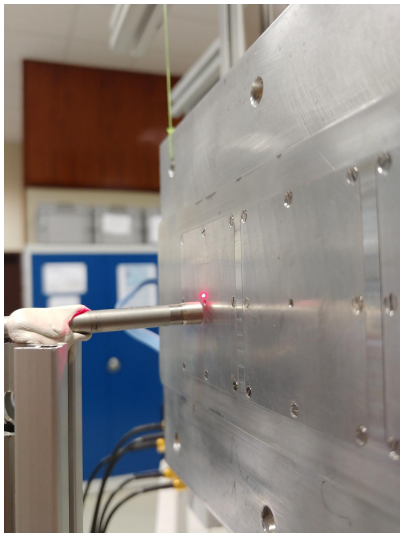

(c)

Figure 3: Pictures of the complete prototype with 5 flush-mounted cells, the electrodynamic shaker for external excitation, the laser vibrometer and the microphone located in cell #1.

The shunt impedance Z connected to the piezoelectric transducer is now defined as a capacitance C_s such that $i = C_s \dot{V}_p$. Then, expression (2) in the Laplace domain becomes:

$$-s\theta X(s) + C_p V_p(s) s = -C_s V_p(s) s \tag{3}$$

with $s = j\omega, s \in \mathbb{C}$ as the Laplace variable and ω the frequency in $rad.s^{-1}$. The displacement of the structure is now:

$$X(s) = \frac{1}{\theta} \left(C_p + C_s \right) V_p \tag{4}$$

It is clear that if C_s is a negative capacitance such that $C_s \approx -C_p$, the displacement $X(s)$ is controlled and tends toward 0. Since the current $i(t)$ in the shunt circuit is directly driven by voltage input u of the current source circuit, the ideal control signal voltage u would be expressed by:

$$u(s) = -K C_p V_p(s) s \tag{5}$$

with $K \in \mathbb{R}^+$ in $[V/A]$ the gain of the impedance control circuit. However, a pure derivative controller is not desirable from a practical point of view and (5) is to be approximated with a stable controller later.

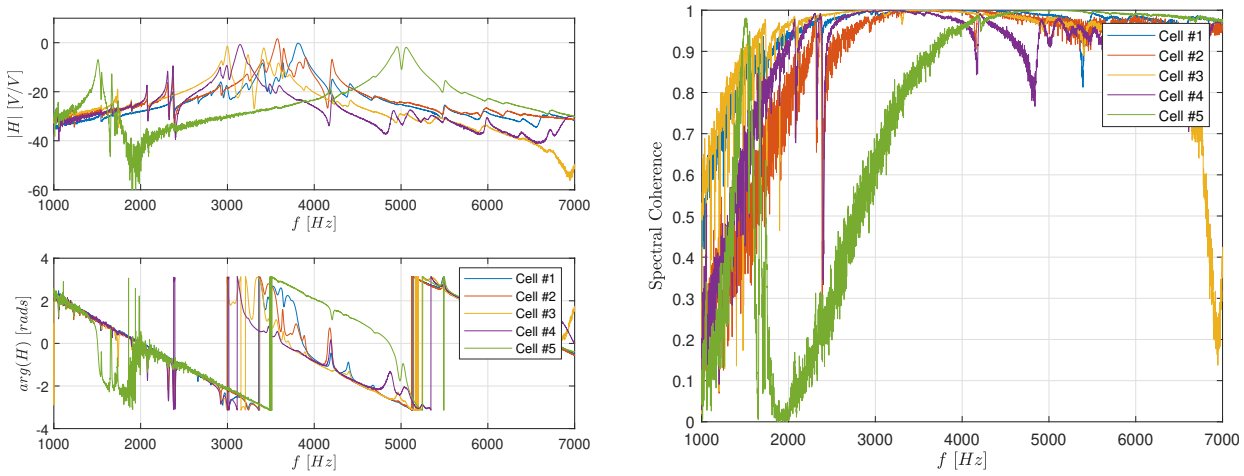

(a) (b)

Figure 4: (a) Measured frequency response functions from DAC signal to vibrometer for each piezoelectric cell (b) Magnitude squared spectral coherence of each measured frequency response function.

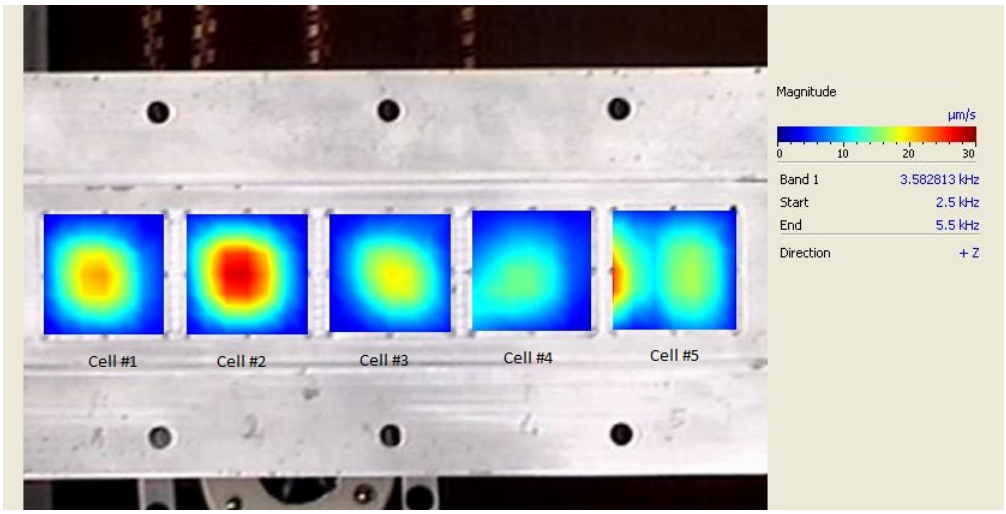

Figure 5: Vibrometer measures of the velocity field at the surface of each piezoelectric cell for a noise excitation as control signal.

3.2 Ideal Negative Capacitance Estimation

Since manufacturing and assembly processes can cause a high level of uncertainties in the electro-mechanical behavior of the cells, it is rather reasonable for this type of smart structure to estimate the ideal negative capacitance controller based on the measured frequency responses of the system.

First, a schematic representation of the control problem is displayed in Figure 7 where 4 main frequency response functions $H_i(f)$ are to be identified for each cell:

- $H_1(f)$ and $H_2(f)$ characterizing respectively the transfers from the voltage control input sent to the Howland current source (DAC) to the actual voltage output of the impedance control circuit (ADC), image of the transducers voltage, and the voltage output from the vibrometer, image of the cell's surface velocity
- $H_3(f)$ and $H_4(f)$ characterizing respectively the transfers from the perturbation *i.e* the shaker voltage

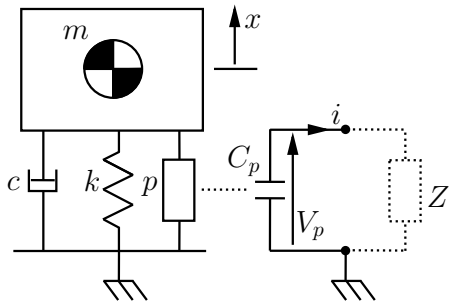

Figure 6: Electro-mechanical model, 2 DOF.

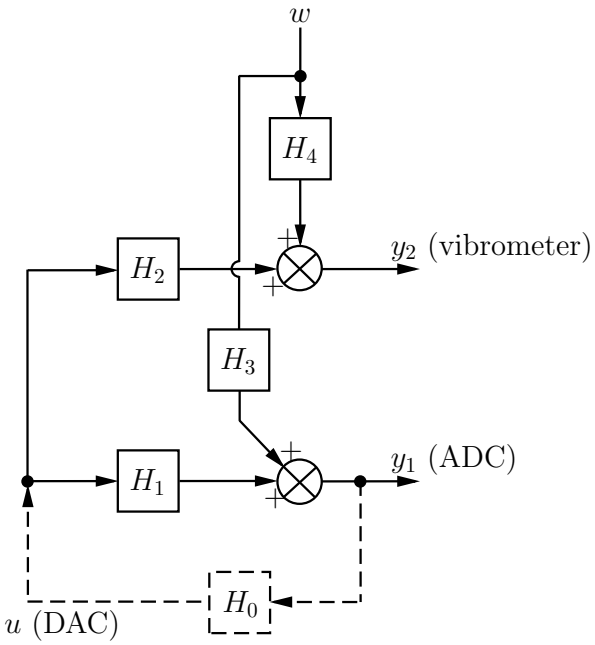

Figure 7: Schematic representation of the control problem for system

input signal w to the actual voltage output of the impedance control circuit, and the voltage output from the vibrometer.

The controller is then defined by $H_0(f)$ where its objective is to control the vibration level *i.e* the transmissibility between the perturbation w and the signal y_2.

The measured frequency response functions for each piezoelectric cell are displayed in Figure 8. First, the measured functions $H_1(f)$ are presented in Figure 8a. It is worth noticing that this FRF is clearly driven by an equation of the form (2) with a major contribution of the electrical part C_p over the entire bandwidth. However, the effects of the electromechanical coupling coefficients θ are still visible on the FRF amplitude and phase close to the cell mechanical modes identified in 4a or 8b(zoom). This observation is absolutely essential since it means that the structure deformation is observable by the transducers, enabling a vibration control strategy based on electrical impedance control. The evident similarities between the Figures 8c and 8d support the previous conclusion by confirming that the transducers observe effectively the structure displacement, as the laser vibrometer. Hence, it is possible to confirm from the presented frequency response functions, the ability of the designed piezoelectric cells to act as sensors and actuators for an impedance control system.

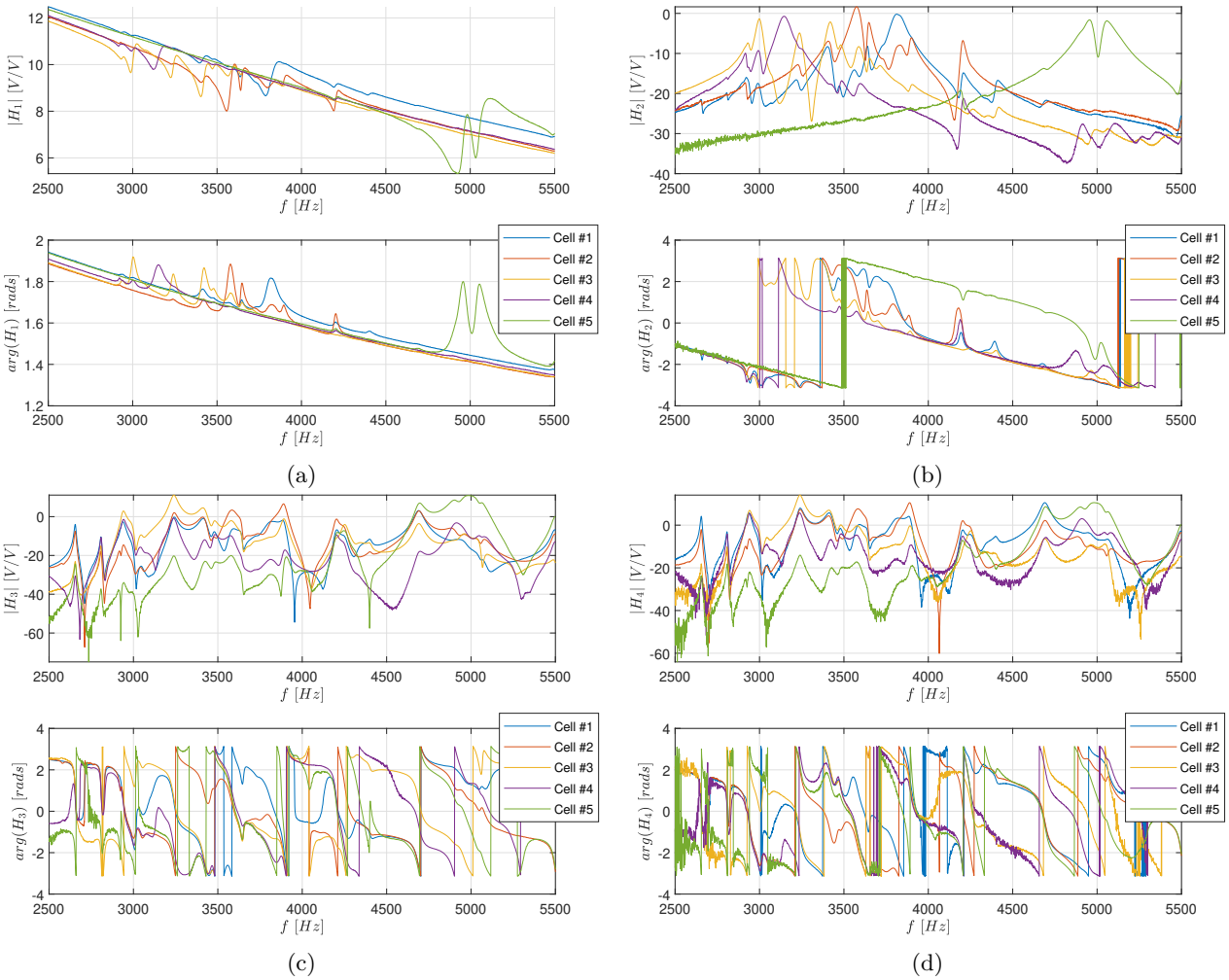

Figure 8: Measured frequency response functions $H_i(f)$ from scheme 7: (a) $H_1(f)$ from impedance control circuit input (DAC) to output (ADC), (b) $H_2(f)$ from impedance control circuit input (DAC) to vibrometer signal, (c) $H_3(f)$ from external excitation (shaker) to impedance control circuit output (ADC), (d) from external excitation (shaker) to vibrometer signal.

Let us now express the cell voltage output as a function of the perturbation:

$$\begin{aligned} Y_1(s) &= H_3(s)W(s) + H_1(s)U(s) && (6)\\ &= H_3(s)W(s) + H_1(s)H_0(s)Y_1(s) && (7)\\ &= (I - H_1(s)H_0(s))^{-1} H_3(s)W(s) && (8) \end{aligned}$$

Then, the vibrometer signal can be written as:

$$\begin{aligned} Y_2(s) &= H_4(s)W(s) + H_2(s)U(s) && (9)\\ &= H_4(s)W(s) + H_2(s)H_0(s)Y_1(s) && (10)\\ &= \left(H_4(s) + H_2(s)H_0(s)\left(I - H_1(s)H_0(s)\right)^{-1} H_3(s)\right) W(s) && (11) \end{aligned}$$

We now define the function $H_c(s)$ to minimize through the controller that expresses the effect of $H_0(s)$ on

the reference transmissibility $Y_2(s)/W(s)$ such that:

$$H_c(s) = Y_2(s)/\left(W(s)H_4(s)\right) \quad (12)$$

$$= I + H_2(s)H_0(s)\left(I - H_1(s)H_0(s)\right)^{-1} H_3(s)H_4(s)^{-1} \quad (13)$$

Finally, the functions $H_{c,j}(f)$ are computed between $2.5kHz$ and $5.5kHz$ for each cell j, with a controller $H_{0,j}(s)$ of the form (5) such that:

$$H_{0,j}(s) = -k_j s \quad (14)$$

with $k_j \in \mathbb{R}^+$. Different values of the gain k_j are explored to determine the optimal equivalent negative capacitance controller. In addition, a discrete criteria function $\alpha_j(k_j)$ is defined to quantify the effect of the control on $H_{c,j}(f)$ such that:

$$\alpha_j = \sum_{f=2.5\times10^3}^{f=5.5\times10^3} 20 \times log10\left(|H_{c,j}(f)|\right) \quad (15)$$

Thus, the reference value for the proposed criteria is $\alpha_j(0) = 0$ (no control applied). The results of this parametric study on the control gains k_j are presented in the Figure 9.

Since the impedance control circuit can induce some time delay between the voltage control input and the actual current signal in the transducers, another parametric study is conducted to estimate the optimal phase shift of the controller expression (14). Hence, once the optimal gain $k_{j,opt}$ is determined for each cell, the following controller is applied to the simulated system:

$$H_{0,j}(s) = -k_{j,opt}\boldsymbol{e}^{i\phi_j} s \quad (16)$$

for different values of phase shift ϕ_j to obtain the optimal phase shift $\phi_{j,opt}$ for each cell. It is worth noticing that $\phi_{j,opt}$ shall be small and negative to ensure the final controller is stable and still correspond to a negative capacitance control. The final results of the performed parametric studies on each cell are synthesized in the Table 1.

Cell number	$k_{j,opt}$	$\phi_{j,opt}$ $[deg]$
#1	1.4×10^{-5}	-4
#2	1.5×10^{-5}	0
#3	1.5×10^{-5}	-4
#4	1.5×10^{-5}	-10
#5	1.3×10^{-5}	0

Table 1: Parametric studies: optimal gains and phase shifts on each piezoelectric cell.

From the Figures 9a, 9b and 9c, it is possible to predict that the negative capacitance control will achieve a good level in terms of vibration reduction within the authority bandwidth of the piezoelectric cells #1 to #3 *i.e.* between 3500 and $4000Hz$. However, the piezoelectric cell #4 (see Figure 9d) has a lower electro-mechanical coupling coefficient and thus reduced performances can be expected. Finally, the Figure 9e confirms that the bandwidth of maximum authority for the piezoelectric cell #5 is around 5000Hz and that as for cell #4, a limited effect of the negative capacitance control is expected.

3.3 Controllers synthesis

Now, the ideal negative capacitance controller $H_{0,j}(s) = -k_{j,opt}\boldsymbol{e}^{i\phi_{j,opt}} s$ obtained for each piezoelectric cell must be approximated with a more suitable expression $\hat{H}_{0,j}(s)$ of the controller for real time experiments. Thus, the new proposed controller is expressed by:

$$\hat{H}_{0,j}(s) = \frac{-R_0 k_{j,opt} s + 1}{-R_0 R k_{j,opt} s + R_0 + R} \times \frac{s}{u + vs} \quad (17)$$

where $R_0 < 0$ and $|R_0| \to \infty$ is a virtual negative electrical resistance placed in parallel with the negative capacitance $-k_{j,opt}$, $R < 0$ and $|R| \to 0$ is a virtual negative electrical resistance placed in series with the capacitance $-k_{j,opt}$ and the resistance R_0. Besides, the correction terms u and v are computed such that the desired phase shift $\phi_{j,opt}$ is achieved at $f_c = \omega_c/(2\pi) = 3000Hz$ (start of the control bandwidth). Hence, u and v are written as:

$$u = Re\left\{\frac{-R_0 k_{j,opt} i\omega_c + 1}{-R_0 R k_{j,opt} i\omega_c + R_0 + R} \times \frac{1}{H_{0,j}(i\omega_c)}\right\} \tag{18}$$

$$v = -\omega_c Im\left\{\frac{-R_0 k_{j,opt} i\omega_c + 1}{-R_0 R k_{j,opt} i\omega_c + R_0 + R} \times \frac{1}{H_{0,j}(i\omega_c)}\right\} \tag{19}$$

with $R_0 = -1e10$ and $R = -0.5$. The value of R_0 is chosen such that $MAX|\lambda(\hat{H}_{0,j})| < 1.25 \times 10^5$ which is a hardware limitation due to the sampling frequency of the controller ($50kHz$). R is chosen only to guarantee the stability of the controller *i.e* $MAX\{Re\{\lambda(\hat{H}_{0,j})\}\} < 0$.

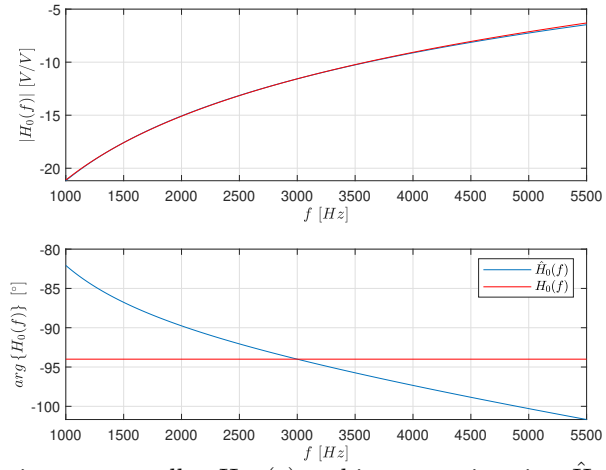

Figure 10: Ideal negative capacitance controller $H_{0,j}(s)$ and its approximation $\hat{H}_{0,j}(s)$ for real time experiments.

The Figure 10 displays the piezoelectric cell #1 controller as an example to illustrate $H_{0,j}(s)$ and $\hat{H}_{0,j}(s)$. One can observe on this figure that the gains are similar between the two compared transfer functions. As for the phase, the real controller $\hat{H}_{0,j}(s)$ has the desired phase at $3kHz$ by definition and a phase error inferior to $10°$ until $5kHz$ which should be small enough to control properly the piezoelectric cells within this frequency bandwidth.

4. CONTROL RESULTS

Finally, the designed controllers are implemented using a dSPACE MicroLabBox controller running at a sampling frequency of $50kHz$. The prototype containing the 5 piezoelectric cells is excited dynamically with an electrodynamic shaker and the vibration level is measured at the center of the skin surface for each cell with the laser vibrometer PSV400. In addition, a microphone B&K is also placed perpendicularly to the cells at each measure, at approximately 3 to 4 mm to the center of the skin surface. The objective is to measure also the acoustic emission of the system and confirm that the cell prototypes show sufficient vibroacoustic coupling also for noise control applications.

The results obtained are displayed in the Figures 11 and 12 where the effect of the controllers $\hat{H}_{0,j}$ is visible on the power spectral densities (PSD) of the vibrometer signal and microphone signal for each cell. The controlled bandwidth for the cells #1 to #4 is $[3200 - 3800]Hz$ and $[4100 - 5000]Hz$ for cell #5. The average attenuation level on each sensor is also computed for these frequency bands and summarized in Table 2.

Cell number	Bandwidth	Vibrometer	Microphone
#1	$[3200-3800]Hz$	-7.8	-8.3
#2	$[3200-3800]Hz$	-5.3	-4.5
#3	$[3200-3800]Hz$	-7.3	-7.1
#4	$[3200-3800]Hz$	-4.6	-7.5
#5	$[4100-5000]Hz$	-7.6	-4.9

Table 2: Control results on the PSD: average attenuation level on each sensor for the considered bandwidths.

One can notice immediately that as expected, the designed controller based on the negative capacitance principle provides an interesting reduction of the vibration level within the authority bandwidth of the piezoelectric cell, which is especially observable on the cells #1, #2, and #3.

Despite the simplicity of the controller, the spillover effect outside the control bandwidth is limited thanks to the modal character of the control. Indeed, the transducers have no controllability on the structure outside the authority bandwidth and thus affect only marginally the vibration level. In addition, active impedance control of transducers allows achieving collocated control, thus reducing parasitic effects of phase errors within the closed-loop.

It is very interesting to observe the close similarity in the PSD between the vibrometer and the microphone. It confirms that a sufficient vibroacoustic coupling is achieved between the cell's surface and the air. Hence, the noise level emitted by the prototype excited dynamically is also controlled within the same proportions as the vibration level.

As identified previously, the results from the cell #5 are shifted in frequency compared to the 4 other cells due to different boundary conditions. Still, the negative capacitance controller manages to reduce both the vibration and noise level with reasonable performance.

4.1 Discussion

A reasonable attenuation level has been achieved here by the proposed negative capacitance controller. Though, it is essential to recall that no external sensors are used within the closed-loop, only the transducers voltage. Hence, each piezoelectric cell acts both as a deformation sensor and a mechanical actuator, guaranteeing maximum controllability of the system. The designed prototype, functional as a stand-alone vibration and noise controller, is a successful preliminary step towards integrated flush-mounted cells in aerodynamic profiles. Hence, the future experiments will consist in placing the proposed prototype on a profile inside a wind tunnel and continue the development of the control laws for the reduction of vibration and noise in the presence of external acoustic sources and turbulent airflow. Thus, the present results can be considered promising since they confirm the ability of the proposed design to control the vibrations on a certain bandwidth and also have authority on the acoustic field around the profile.

5. CONCLUSION

The present manuscript proposed a preliminary research work on the control of flush-mounted piezoelectric cell prototypes intended to be integrated at the surface of aerodynamic profiles to control the vibration and noise induced by turbulent airflow. To achieve this objective, the piezoelectric transducers of each cell were controlled using a numerical equivalence to a negative capacitance controller within their maximum controllability bandwidth, corresponding to each cell's main electro-mechanical mode. Hence, an average reduction level of $-6dB$ has been achieved on a minimum bandwidth of $600Hz$ around the identified electro-mechanical modes on both the vibration level and noise level emitted by the mechanical structure, confirming the performance of negative capacitance control. These early results are promising and provide sufficient confidence for the next step, consisting in placing the actual prototype in a stator vane profile inside a wind tunnel with turbulent airflow and an external acoustic source to develop further the impedance control laws.

ACKNOWLEDGMENTS

The InnoSTAT project has received funding from the Clean Sky 2 Joint Undertaking (under grant agreement No 865007 The JU receives support from the European Union's Horizon 2020 research and innovation program and the Clean Sky 2 JU members other than the Union. This publication reflects only the author's view and the JU is not responsible for any use that may be made of the information it contains.

REFERENCES

[1] Hagood, N.W. and Von Flotow, A., 1991. *Damping of structural vibrations with piezoelectric materials and passive electrical networks*. Journal of sound and vibration, 146(2), pp.243-268.

[2] Preumont, A., 2018. *Vibration control of active structures: an introduction* (Vol. 246). Springer.

[3] Cross, C.J. and Fleeter, S., 2002. *Shunted piezoelectrics for passive control of turbomachine blading flow-induced vibrations. Smart materials and Structures*, 11(2), p.239.

[4] Hohl, A., Neubauer, M., Schwarzendahl, S.M., Panning, L. and Wallaschek, J., 2009, April. *Active and semiactive vibration damping of turbine blades with piezoceramics*. In Active and Passive Smart Structures and Integrated Systems 2009 (Vol. 7288, pp. 554-563). SPIE.

[5] Duffy, K.P., Choi, B.B., Provenza, A.J., Min, J.B. and Kray, N., 2013. *Active piezoelectric vibration control of subscale composite fan blades*. Journal of engineering for gas turbines and power, 135(1).

[6] Behrens, S., Fleming, A.J. and Moheimani, S.O.R., 2003. *A broadband controller for shunt piezoelectric damping of structural vibration*. Smart materials and structures, 12(1), p.18.

[7] Moheimani, S.R. and Fleming, A.J., 2006. *Piezoelectric transducers for vibration control and damping*. Springer Science & Business Media.

[8] Yu, H., and Wang, K. W. (May 21, 2007). *Piezoelectric Networks for Vibration Suppression of Mistuned Bladed Disks*. ASME. J. Vib. Acoust. October 2007; 129(5): 559–566. https://doi.org/10.1115/1.2775511

[9] Zhang, J.M., Chang, W., Varadan, V.K. and Varadan, V.V., 2001. *Passive underwater acoustic damping using shunted piezoelectric coatings*. Smart materials and structures, 10(2), p.414.

[10] Perez, M., Ezzine, M., Billon, K., Clair, V., Mardjono, J. and Collet, M., 2020, September. *Design and Optimization of Piezoelectric Actuators for Aeroacoustic Noises Control in a Turbofan*. In Smart Materials, Adaptive Structures and Intelligent Systems (Vol. 84027, p. V001T02A010). American Society of Mechanical Engineers.

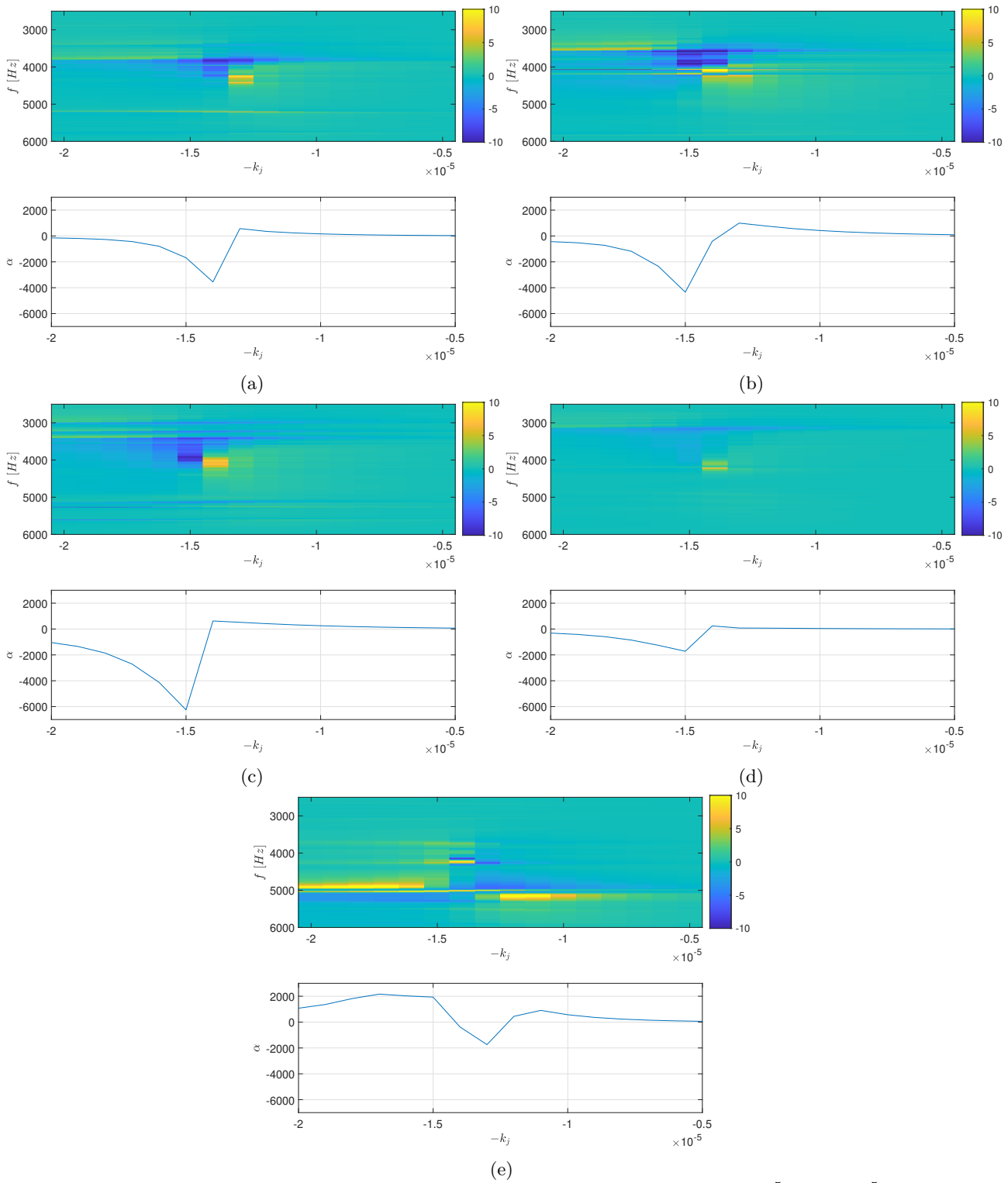

Figure 9: Computed functions $H_{c,j}(f)$ and $\alpha_j(k_j)$ for each cell j with $k_j \in [0.5 \times 10^{-5} : 2 \times 10^{-5}]$: (a) cell #1, (b) cell #2, (c) cell #3, (d) cell #4, (e) cell #5.

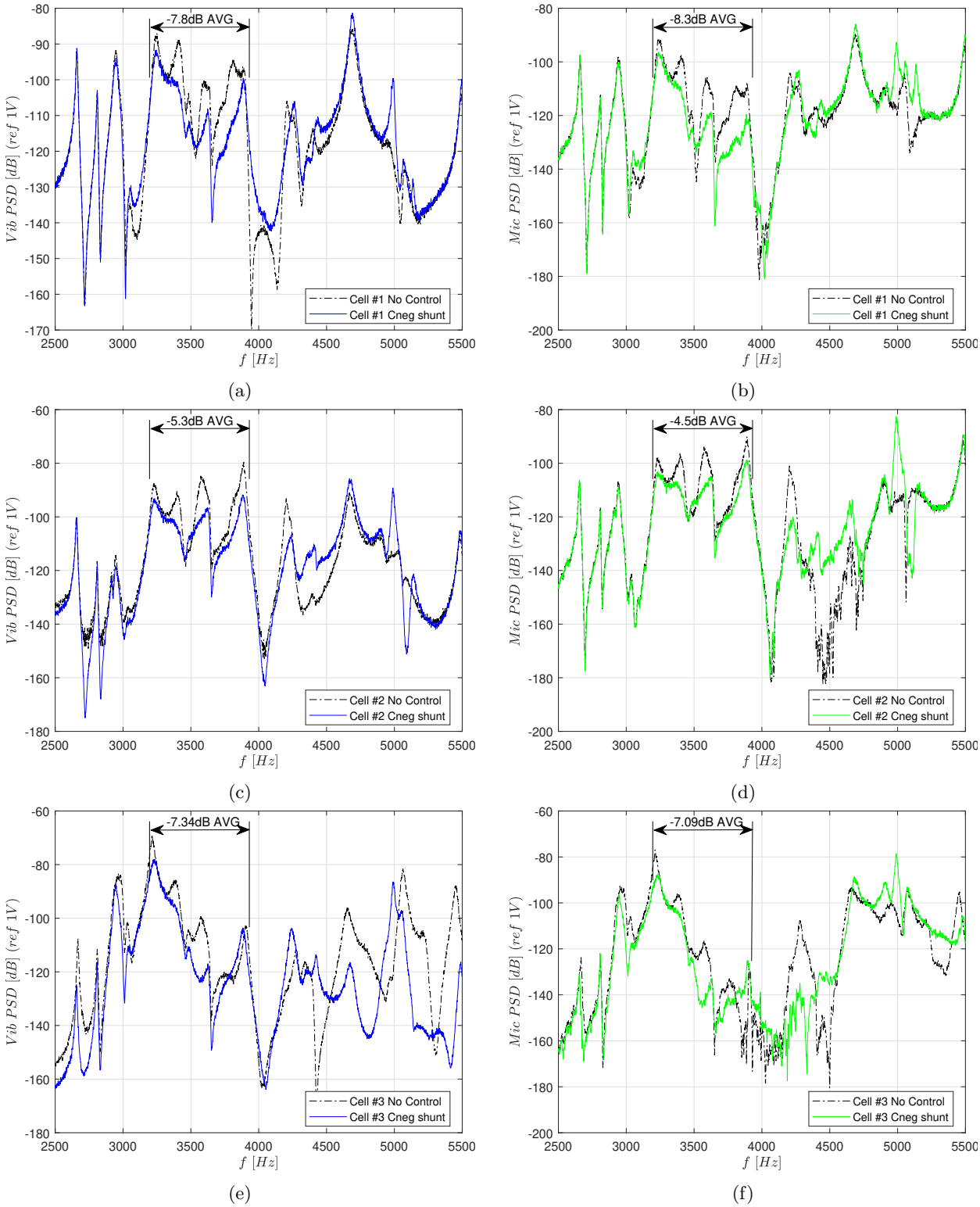

Figure 11: Control results on the PSD: #cell 1 (a) vibrometer and (b) microphone, #cell 2 (c) vibrometer and (d) microphone, #cell 3 (e) vibrometer and (f) microphone.

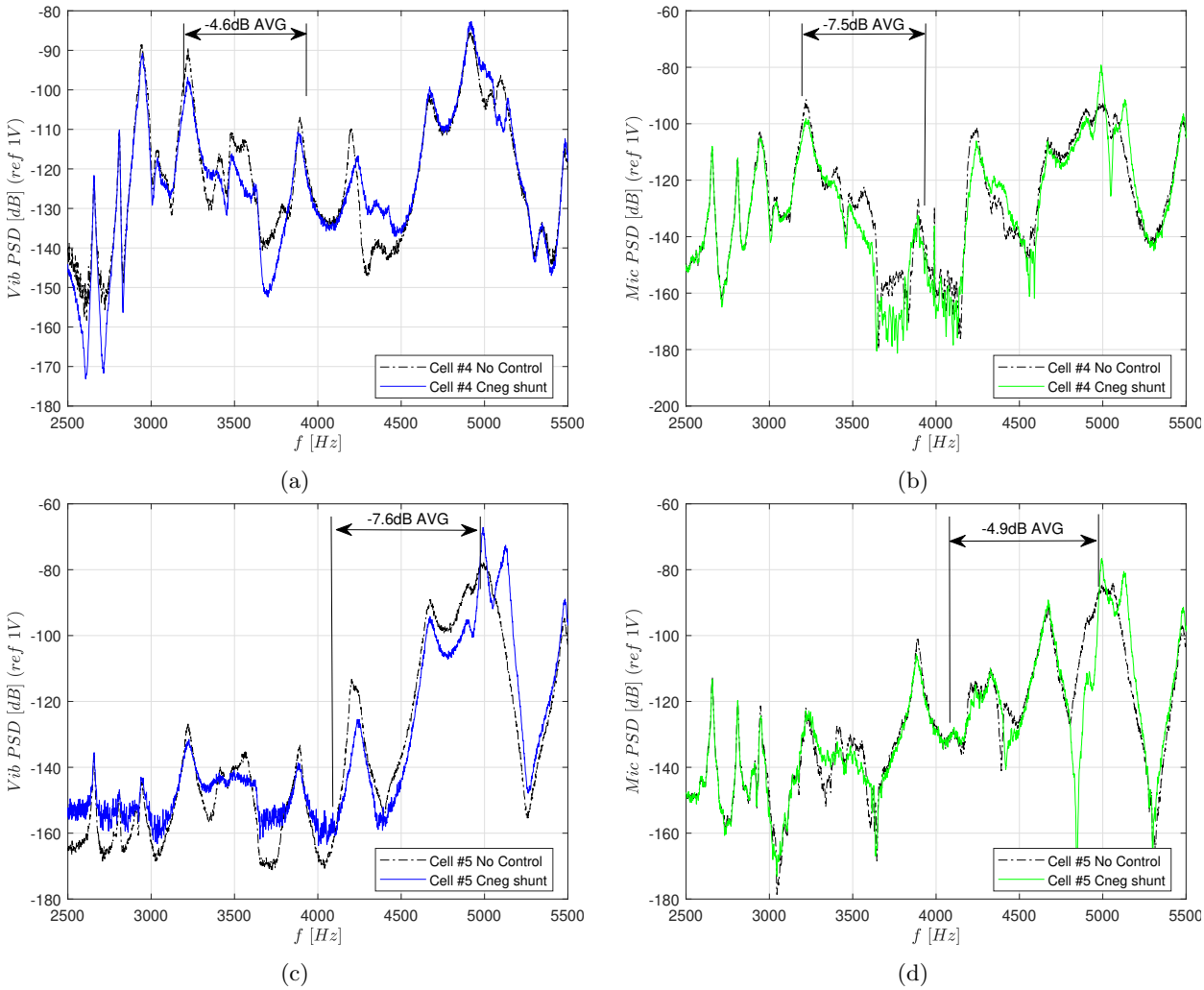

Figure 12: Control results on the PSD: #cell 4 (a) vibrometer and (b) microphone, #cell 5 (c) vibrometer and (d) microphone.